Light localisation and magneto-optic enhancement in Ni anti-dot arrays

Markus Rollinger,[†] E. Melander,[‡] Philip Thielen,[†] Erik Östman,[‡] Vassilios Kapaklis,[‡] Mirko Cinchetti,[†] Antonio Carcia-Martin,[¶] Martin Aeschlimann,[†] and E.Th. Papaioannou[*,†]

Fachbereich Physik and Forschungszentrum OPTIMAS, Technische Universität Kaiserslautern, 67663 Kaiserslautern, Germany, Department of Physics and Astronomy, Uppsala University, Box 516, SE-75120, Uppsala, Sweden, and IMM-Instituto de Microelectronica de Madrid (CNM-CSIC), Isaac Newton 8, PTM, Tres Cantos, E-28760 Madrid, Spain

E-mail: papaio@rhrk.uni-kl.de

Phone: +49 (0) 631 205 4099. Fax: +49 (0)631 205 4095

Abstract

The presence of surface plasmons in magnetic nano-structures can strongly influence the magneto-optical properties of the magnetic materials. Here, we show with the help of photoemission electron microscopy how the light is localised on the patterned magnetic surface. We reveal by using different energies and polarisation states of incident light that light is concentrated in spots that form an hexagonal lattice or it forms lines perpendicular to incident polarisation direction of light. These effects are measured only at energies where excitations

[*]To whom correspondence should be addressed

[†]Fachbereich Physik and Forschungszentrum OPTIMAS, Technische Universität Kaiserslautern, 67663 Kaiserslautern, Germany

[‡]Department of Physics and Astronomy, Uppsala University, Box 516, SE-75120, Uppsala, Sweden

[¶]IMM-Instituto de Microelectronica de Madrid (CNM-CSIC), Isaac Newton 8, PTM, Tres Cantos, E-28760 Madrid, Spain

of surface plasmons are expected. We show that the light localisation on the patterned surface defines the enhancement of the polar magneto-optical Kerr effect.

Introduction

The field of magneto-plasmonics is growing rapidly nowadays with the main aim to explore the combination of magnetic and plasmonic functionalities in patterned nano structures.[1] In particular, metallic antidot arrays are famous for their ability to enhance optical transmission due to their capability to sustain surface plasmons polaritons (SPPs).[2] SPPs have higher in-plane momentum than the incident light, however are excited in such patterns due to momentum transfer provided by antidot lattice.[3] In our study, the patterned layer is composed of hexagonal arrays of holes of $d = 275$ nm diameter and $a = 470$ nm pitch size. If a magnetic material forms the pattern then the interaction of surface plasmons and magnetic materials can reveal very interesting effects. In particular, the excitation of SPPs has been found to enhanced the polar magneto-optical Kerr effect (P-MOKE) signal in Ni,[4,5] Fe,[6] Co[7] films, as well as in hybrid structures composed of noble and magnetic metals/dielectrics such as Au and Co/Iron garnets.[8,9] SPPs have been also shown to influence the transverse magneto-optic response TMOKE.[4] Furthermore, the magnetic field can be also used to modify the dispersion relation of Spps as it has been recently shown in a interferometer like structure composed of trilayers of Au/Co/Au.[10]

In spite of the numerous studies on the plasmonic behavior of magneto-plasmonic lattices and the enhanced magneto-optical signal, the mechanism of coupling between plasmonic and magneto-optic properties is not clarified yet. Recent first studies in this direction on dots have shown the interaction of localized plasmons in magnetic nanoislands caused either a phase change in the magnetooptical signal[11] or increased the pure magneto-optical conversion factor leading to an enhancement of the PMOKE signal.[12] Furthermore, in the non-linear optical regime the excitation of a surface plasmon at an interface of Co antidot film has shown not only to enhance the second-harmonic generation (SHG) efficiency, but also to activate a quadrupole nonlinear-optical

mechanism.[13]

Here we elucidate further the mechanisms of coupling between plasmonic and magneto-optic properties for the case of antidot patterns. With photo-emission electron microscopy images and by using incident light of different energies and polarization states we visualise the light localisation on the patterned surface. Remarkable different images are recorded at energies where SPPs are expected. The localisation of light at the plasmonic resonances leads to a significant increase of the pure magneto-optical conversion that drives the enhancement the magneto-optic response of the patterned magnetic material.

Results and discussion

Reflectivity and plasmonic resonances

The patterned sample under study has holes of $d = 275$ nm diameter. The distance from hole center to hole center is $a = 470$ nm. The Ni film of 100 nm thickness was grown on Si substrate on top of a seed Ti layer of 2nm thickness. The Ni film is covered with a protective layer a very thin Au layer of 2 nm. Reflectivity spectra were recorded with different polarisation states of light for the Ni anti-dot sample and for a Ni reference continuous film of the same thickness. The reflectivity measurements were recorded at 6.5 $^\circ$ angle of incidence and without an application of a magnetic field. Important to note here is that initially the plane of incidence was aligned along the nearest neighbours direction of the hexagonal lattice (small deviations can not be excluded though when positioning the sample in different setups). The light polarization was then rotated from p- to s-type.

Fig.1 (top graph) reveals the relative reflectivity curves for s- and p- light for the patterned sample. The reflectivity is normalised relative to the reflectivity of the Ni continuous film. Drops in reflectivity for the patterned sample are observed for both s- and p-polarization at specific energies. The minima of reflectivity are correlated to the surface plasmon excitation at metal/air interface. Fig.1 (lower graph) shows the calculated dispersion curves of surface plasmons. The calculation

of the resonant excitations is based on the momentum matching condition between incident light and lattice geometry:

$$\overrightarrow{\mathbf{k}}_{spp} = \overrightarrow{\mathbf{k}}_x \pm i\overrightarrow{\mathbf{G}}_x \pm j\overrightarrow{\mathbf{G}}_y \quad (1)$$

where k_{spp} is the surface plasmon polariton wave vector, $k_x = k_0 sin\theta$ is the component of the incident wave vector that lies in the plane of the sample, $\overrightarrow{\mathbf{G}}_x$, and $\overrightarrow{\mathbf{G}}_y$ are the basis vectors of the reciprocal hexagonal lattice and i, j are integers.

Such coupling gives rise to the so-called Bragg surface plasmons. The different dispersion curves correspond to different orders (i,j) of the Bragg plasmons resonances. The modes present here for p-light are the : (i,j) (-1,0)-(0,-1),/ (1,-1)-(-1,1)/ and (1,0)- (0,1). The calculation reveals different modes for s-polarization excitation (not shown): (0,-1)/ (-1,0)-(1,-1)/ ((1,0)-(-1,1) and also the (0,1) mode. The different modes have also different magnitudes of Reflectivity as the color coding indicates. The drawn lines indicate the intersection of reflectivity minima with the dispersion curve of surface plasmon for the given angle of incidence. The very good agreement between theory and experiment (also for the s-polarized light) confirm the origin of reflectivity minima due to the excitation of surface plasmons on our magneto-plasmonic structure.

Photo-emission electron microscopy on the magneto-plasmonic structure

To elucidate further the role of excitation of SPPs on such magneto-plasmonic structure, Photo-Emission Electron Microscopy (PEEM) was used. PEEM is a powerful technique able to image the photoelectron distribution of the sample on a nanometer local scale. Furthermore, the electrostatic lens system offers a spatial resolution of 25 to 30 nm, beyond the optical diffraction limit, and is well-suited to image the electron distribution within our nm-scaled anti-dot structure. By using as light sources for the microscope a mode-locked Ti:Sapphire laser oscillator with a photon energy of $\hbar\omega = 1.55$ eV and its frequency-doubled fundamental mode with a photon energy of $\hbar\omega = 3.10$ eV as well as a commercial optical parametric oscillator we were able to achieve variable photon

energies between 1.65 eV and 3.59 eV. Worth also to note here is that the angle of incidence of the laser light impinging on the sample surface was also 4° relative to the surface normal, that is similar to the one used for the polar Kerr rotation measurements. This will allow us later to directly compare the PEEM experiment with the magneto-optical activity of the sample. Here as well as before slightly misalignment between the incident plane and the nearest neighbour direction can not be rule out between the different experiments.

Initially we started with incident p-polarized light aligned along the direction of the nearest neighbouring holes in the real space (ΓK direction in the reciprocal space). As it is known, P-polarized light is defined when the polarization is aligned parallel to the plane of incidence (and thus has an in-plane as well as an out-of-plane component on the sample surface). However here, the 4° angle of incidence renders the out-of-plane component very small. The bigger part of the projection of p-polarized light lies in-plane on the sample surface and parallel to the nearest neighbouring direction. Then we gradually rotated the polarization with the help of a retardation plate eventually having s-polarized light. In this case the polarization axis is on the sample surface but parallel now to the direction of the next nearest neighbours (ΓM direction in reciprocal space).

In Fig.2 we present PEEM images recorded at different energies of incident light. PEEM measures the number of the emitted electrons from a sample surface. In our case, we expect that if Spps are present as a result of the coupling of the incident light with the periodic lattice then this will enhance the electric field. If the electric is reinforced then we expect to measure with PEEM images with an increased intensity due to the enhanced number of the emitted electrons. The top two images in the first row of the Fig.2 are used as references (taken at energy of 1.55 eV and UV). The microscope is imaging just the pattern structure. Some bright spots on the sample surface are just non-wished particles agglomerations. The next three rows of Fig.2 shows images of the detected electron intensity with the use of p- or s- polarized light at characteristic energies.

Initially we show the results for the energy of 2.4 eV. Weak emission is observed from different areas of the surface that is not dependent on the polarization state of light. This can be understood as normal emission since the energy is enough to get some PEEM intensity from the sample

surface.

The behaviour is changing dramatically at 3.1 eV (third row): PEEM images show now strong spot like emission and continuous lines patterns. In particular, when the incident E-field is parallel to the next neighbours (p-light) PEEM images revealed dot like emission from the sample surface. The spots are formed around the holes and they are also arranged in an hexagonal pattern. This behaviour is repeated every 60 degree rotation of the polarization state of light. When E-field is parallel to the next nearest neighbours (s-light) a big change in the Peem images is observed. Now bright continuous lines are formed perpendicular to the polarization direction of light. The created emission lines are covering the material space and not the holes. The pattern is also repeated every 60 degrees rotation of polarization mirroring the symmetry of the structure. The energy of 3.1 eV is very close to the excitation energy of Spps for both s, and p-light. The last row shows PEEM images recorded at $\hbar\omega = 3.4$ eV. The intensity patterns exhibits similar behaviour: hexagonal bright spot formation for p-pol and continuous lines perpendicular to the next nearest direction for s-light are seen. The energy of 3.4 eV is also close a plasmonic resonance, however of different order (see Fig.1).

In order to understand the origin of the photoelectrons and thus the near-field distribution of the exciting light in the PEEM measurements, we compare the measured photoemission pattern to near-field simulations. Those simulations are performed with a commercial-grade simulator based on the finite-difference time-domain method (Lumerical FDTD Solutions, www.lumerical.com). The design of the simulated structure is the same as the magneto-plasmonic sample accounting for the layered structure including substrate, buffer layer, Ni film and Au capping layer. As excitation source for the simulations shown here we use a plane-wave source with 3.1 photon energy. The field distribution is recorded within the 2 thick Au capping layer. Figure 3 compares the experimental photoemission patterns for different polarization angles ranging from 0ř to 90ř recorded at energy of 3.1 eV to a logarithmic plot of the electrical field magnitude obtained by the numerical calculations. In general, a very good agreement is apparent. For p-polarized light the electrical field vector is pointing along the horizon, approximately aligned with the direction of nearest

neighbouring holes. A hexagonal lattice of dots is visible in the photo-emission pattern. The simulated near-field intensity distribution delivers locally confined spot-like maxima exhibiting the same hexagonal symmetry inside the material located between neighboring holes connected by the direction of the E-field vector. A counter-clockwise rotation of the polarization axis by 30ř yields a completely different photo-emission pattern. Instead of hexagonal dots we observe a broader distributed stripe pattern. Once again, the simulation is in good agreement showing broad linear maxima of the electric field between the holes. The stripes are aligned perpendicular to the electric field vector. When the polarization axis is rotated by a total of 60ř, corresponding to the symmetry of the hexagonal antidot lattice of the sample, the PE image shows again a spot-like pattern. Comparing the spot-like pattern to the first image, one can clearly see a shift in position (see the blue boxes inserted into the images as a guide to the eye). This is in accordance to the simulated near-field distribution which shows the localized spots between neighbooring holes along the direction of the E-field vector. The shift in position is directly reproduced. Due to the symmetry of the sample, a rotation of the polarization axis by a total of 90ř (s-polarized light) shows a similar situation as a rotation by 30ř. The PE pattern as well as the simulation show a stripe-like pattern, where the stripes are aligned perpendicular to the E-field vector. In conclusion, comparing the photoemission pattern to the simulations provides the understanding of the polarization-dependent near-field distribution. Whenever the electrical field vector is aligned parallel to the nearest neighbours the near-field distribution shows a locally confined spot-like pattern. Owing to the orientation of the hole lattice relative to the plane of incidence this corresponds to p-polarized light. In contrast, when the electrical field vector is aligned along the next-nearest neighbors, the near-field is more distributed, forming lines perpendicular to the E-field vector. This represents the case of s-polarized light in our experiments.

Very important to note here is that the E-field was also recorded at several heights in the simulation, 5nm above the whole structure, exactly in the middle of the 2nm Au layer (thus, 1nm below the sample surface) as shown in Fig. 3 and in the middle of the 100nm thick Ni film.There is almost no qualitative difference between the Au and Ni monitor, we see the same dot-like and stripe-like

pattern there, depending on the light polarization.

Correlation of Photo-emission electron microscopy and magneto-optic enhancement

The dramatic changes in the field intensity patterns recorded by PEEM can be correlated to the magneto-optic Kerr response of the structure. Fig.4 shows the polar Kerr rotation spectra for different polarisation states of the incident light. Spectra are recorded for the anti-dot sample and simultaneously for a reference continuous film of the same thickness and composition. The Polar Kerr experiment was performed at 4° angle of incidence similar to the PEEM experiment and at the magnetic saturation of the samples. As in the PEEM experiments, the plane of incidence was aligned along the nearest neighbours direction of the hexagonal lattice. The magneto-optic Kerr effect appears when an p-polarized component (or s-) is present in the reflection from incident s-polarized light (or p-). The complex Kerr rotation $\tilde{\Theta}$ can be related to the corresponding Fresnel reflection coefficients (r_{pp}, r_{ss}, r_{ps}, r_{sp}) with the help of:

$$\tilde{\Theta} = \theta_{\mathbf{K}} + \imath\eta_{\mathbf{K}} = \frac{\mathbf{r}_{sp}}{\mathbf{r}_{pp}} \tag{2}$$

where η_K is the polar Kerr ellipticity and θ_K defines the polar Kerr rotation as the tilt angle of the polarization plane with respect to the incident light. The value of the Kerr rotation can be influenced by two factors:[1,14,15] the intrinsic magneto-optically active electronic transitions (r_{sp} polarization conversion- pure magneto-optic contribution) and the extrinsic reflectivity (r_{pp}- pure optical contribution)

Fig.4 reveals a big enhancement of the polar Kerr rotation θ_K with respect to the continuous film for both s- and p- at energies above 2.4 eV. At exactly 2.4 eV the reflectivity values from Fig.1. and the Kerr rotation for both types of polarization types are similar. More interestingly the value of the Kerr rotation is the same also with the reference continuous sample. The theoretical calculations predicts no presence of surface plasmon resonant condition while the PEEM images

present no polarization dependent features.

The first maximum enhancement of the Kerr rotation at energy region of 2.65-2.7 eV is close to the theoretically predicted excitation of SPPs due to the grating coupling. Moving further on the spectrum at 3.1 eV, the experimental measured Reflectivity for p- light at 3.1 eV decreases further due to the resonant condition resulting in an bigger enhancement of the Kerr rotation. The use of s-polarized light shows an increase of the reflectivity with respect to p-pol and an increase of the Kerr rotation compared to the continuous film. However this increase is smaller than for p-light. Another enhancement maximum is located at the energy of 3.4 eV. More interestingly here, the reflectivity for both polarization states is almost the same and the enhanced Kerr rotation values higher for the s-polarized light.

PEEM images recorded at 3.1 eV, and 3.4 have revealed the localisation of light either as stripe lines or as bright spots with respect to polarization state. This spatial distribution of the electric field recorded by PEEM influences the magneto-optic enhancement. We have recorded the intensity of the electric field patterns with the help of the simulations in Fig. 3 for the full spectral range. The corresponding curves are plotted for p- and s-polarized light in Fig.4 (right axis). We see that the electric fields are strongly intensified for both s- and p-light (p-light has much higher intensity) at a spectral region between 2.5 and 3.5 eV. Inside this spectral region we also observed the strong magneto-optic enhancement. This is a proof that the intensification of the electric field generated by the spatial distribution of the generated surface plasmons leads to an increase of pure magneto-optic contribution since it increases the density of states where magneto-optically active electronic transitions take place. In particular r_{sp} can be written as:[1]

$$|r_{\mathrm{sp}}| \propto \langle E_p E_s \rangle d |\varepsilon_{mo}| \tag{3}$$

where d is the thickness of the film, ε_{mo} its magneto-optical constant and $\langle E_p E_s \rangle$ is the mean value of the product of both components of the field inside the MO layer. The enhancement of both components of the electric field shown in Fig.4 increases the pure magneto-optic contribution on the Kerr enhancement.

Still, the good agreement between intensification of electric field and large enhancement for both s-and -p incident polarizations can not fully explain all the observed spectral differences between s- and p-light. We refer for example to the lower Kerr rotation values for s-light around 3.1 eV compare to p-light. These are due to the variation of reflectivity as shown in Fig.1. As discussed above the Kerr rotation also depends on the pure optical contribution. Due to the slightly different angle of incidence the absolute comparison of reflectivity and Kerr spectra is difficult, however approximately still valid. As shown in in Fig.1 the reflectivity which enters as a denominator in the expression of the Kerr rotation, for s- excitation goes through a local maximum around 3.1 eV while the p- excitation reveal a broad minimum. The lower reflectivity of p-excitation results in higher Kerr rotation at this energy.

Conclusions

By recording with PEEM the spatial distribution of electromagnetic fields generated by the surface plasmons and by simulating the field intensity at the location of Ni/Au interface we were able to correlate the enhancement of the polar Kerr effect in a Ni based magneto-plasmonic structure. Peem images have revealed that the use of s- and p- light leads at specific energies to the localisation of light in the form of spots or lines. A hexagonal lattice of dots is visible in the photo-emission pattern for p-excitation, while the rotation of polarization axis by 30,90 $^\circ$ - yields a broader distributed pattern of stripes that are aligned perpendicular to the incident electric field vector. The effects are observed only at energy positions where excitation of surface plasmons is expected. The localization of the electric field results to a significant increase of the field intensity in a spectral region from 2.5 to 3.5 eV. This results in an enhancement of the Kerr rotation due to the increase of the magneto-optical conversion. Significant role to the spectroscopic dependence of the Kerr rotation plays the reflectivity values. Manipulating the Kerr enhancement with s- and p-light around plasmonic resonances open new routes for tailoring the functionality of patterned magneto-plasmonic structures.

Acknowledgement

E.P acknowledges Carl Zeiss Stifftung

Supporting Information Available

Experimental procedures and characterization

The photoelectron distribution of the sample is imaged using a photoemission electron microscope (IS-PEEM, Focus GmbH) located in an ultrahigh vacuum chamber with a base pressure below 10^{-10} mbar. The electrostatic lens system offers a spatial resolution of 25-30nm, beyond the optical diffraction limit, and is well-suited to image the electron distribution within the nm-scaled anti-dot structure. As light sources for the PEEM experiments we use a mode-locked Ti:Sapphire laser oscillator with a photon energy of 1.55 eV and its frequency-doubled fundamental mode with a photon energy of 3.10 eV as well as a commercial optical parametric oscillator providing variable photon energies between 1.65 eV and 3.59 eV. In this experiment the laser light impinges on the sample under an angle of incidence of 4° relative to the surface normal. The polarization axis of the laser light is manipulated by adjusting the angle of a half-wave plate or a variable Berek retarder, respectively, depending on the wavelength in use. That way photoemission images at various photon energies are recorded. The polarization angle is varied between 0 ° (polarization axis pointing horizontally along the nearest neighbour direction of the holes in the sample, also called p-polarized light) and 90 ° (polarization axis pointing vertically along the next-nearest neighbour direction, also called s-polarized light).

This material is available free of charge via the Internet at `http://pubs.acs.org/`.

References

(1) Armelles, G.; Cebollada, A.; GarcÃ■a-MartÃ■n, A.; GonzÃąlez, M. U. *Advanced Optical Materials* **2013**, *1*, 10–35.

(2) Maier, S. A. *Plasmonics: Fundamentals and Applications*; Springer, Berlin, 2007.

(3) Ebbesen, T. W.; Lezec, H. J.; Ghaemi, H. F.; Thio, T.; Wolff, P. A. *Nature* **1998**, *391*, 667–669.

(4) Melander, E.; Ostman, E.; Keller, J.; Schmidt, J.; Papaioannou, E. T.; Kapaklis, V.; Arnalds, U. B.; Caballero, B.; Garcia-Martin, A.; Cuevas, J. C.; Hjörvarsson, B. *Appl. Phys. Lett.* **2012**, *101*, 063107.

(5) Papaioannou, E. T.; Kapaklis, V.; Melander, E.; Hjörvarsson, B.; Pappas, S. D.; Patoka, P.; Giersig, M.; Fumagalli, P.; Garcia-Martin, A.; Ctistis, G. *Opt. Express* **2011**, *19*, 23867–23877.

(6) Papaioannou, E. T.; Kapaklis, V.; Patoka, P.; Giersig, M.; Fumagalli, P.; Garcia-Martin, A.; Ferreiro-Vila, E.; Ctistis, G.

(7) Ctistis, G.; Papaioannou, E.; Patoka, P.; Gutek, J.; Fumagalli, P.; Giersig, M. *Nano Lett.* **2009**, *9*, 1–6.

(8) Martin-Becerra, D.; Gonzalez-Diaz, J. B.; Temnov, V. V.; Cebollada, A.; Armelles, G.; Thomay, T.; Leitenstorfer, A.; Bratschitsch, R.; Garcia-Martin, A.; Gonzalez, M. U. *Appl. Phys. Lett.* **2010**, *97*, 183114.

(9) Belotelov, V. I.; Akimov, I. A.; Pohl, M.; Kotov, V. A.; Kasture, S.; Vengurlekar, A. S.; Venu, G. A.; Yakovlev, D. R.; Zvezdin, A. K.; Bayer, M. *Nature Nanotech.* **2011**, *4*, 1–7.

(10) Temnov, V. V.; Armelles, G.; Woggon, U.; Guzatov, D.; Cebollada, A.; García-Martín, A.; García-Martín, J. M.; Thomay, T.; Leitenstorfer, A.; Bratschitsch, R. *Nature Photon.* **2010**, *4*, 107–111.

(11) Bonanni, V.; Bonetti, S.; Pakizeh, T.; Pirzadeh, Z.; Chen, J.; Nogués, J.; Vavassori, P.; Hillenbrand, R.; Åkerman, J.; Dmitriev, A. *Nano Letters* **2011**, *11*, 5333–5338.

(12) Rubio-Roy, M.; Vlasin, O.; Pascu, O.; Caicedo, J. M.; Schmidt, M.; GoÃśi, A. R.; Tognalli, N. G.; Fainstein, A.; Roig, A.; Herranz, G. *Langmuir* **2012**, *28*, 9010–9020.

(13) Razdolski, I.; Gheorghe, D. G.; Melander, E.; Hjörvarsson, B.; Patoka, P.; Kimel, A. V.; Kirilyuk, A.; Papaioannou, E. T.; Rasing, T. *Phys. Rev. B* **2013**, *88*, 075436.

(14) Papaioannou, E. T.; Meyer, T.; Hillebrands, B. *Journal of Surfaces and Interfaces of Materials* **2014**, *2*, 40?45.

(15) Fumagalli, P.; Munekata, H. *Phys. Rev. B* **1996**, *53*, 15045–15053.

Graphical TOC Entry

Some journals require a graphical entry for the Table of Contents. This should be laid out "print ready" so that the sizing of the text is correct.
Inside the `tocentry` environment, the font used is Helvetica 8 pt, as required by *Journal of the American Chemical Society*.
The surrounding frame is 9 cm by 3.5 cm, which is the maximum permitted for *Journal of the American Chemical Society* graphical table of content entries. The box will not resize if the content is too big: instead it will overflow the edge of the box.
This box and the associated title will always be printed on a separate page at the end of the document.

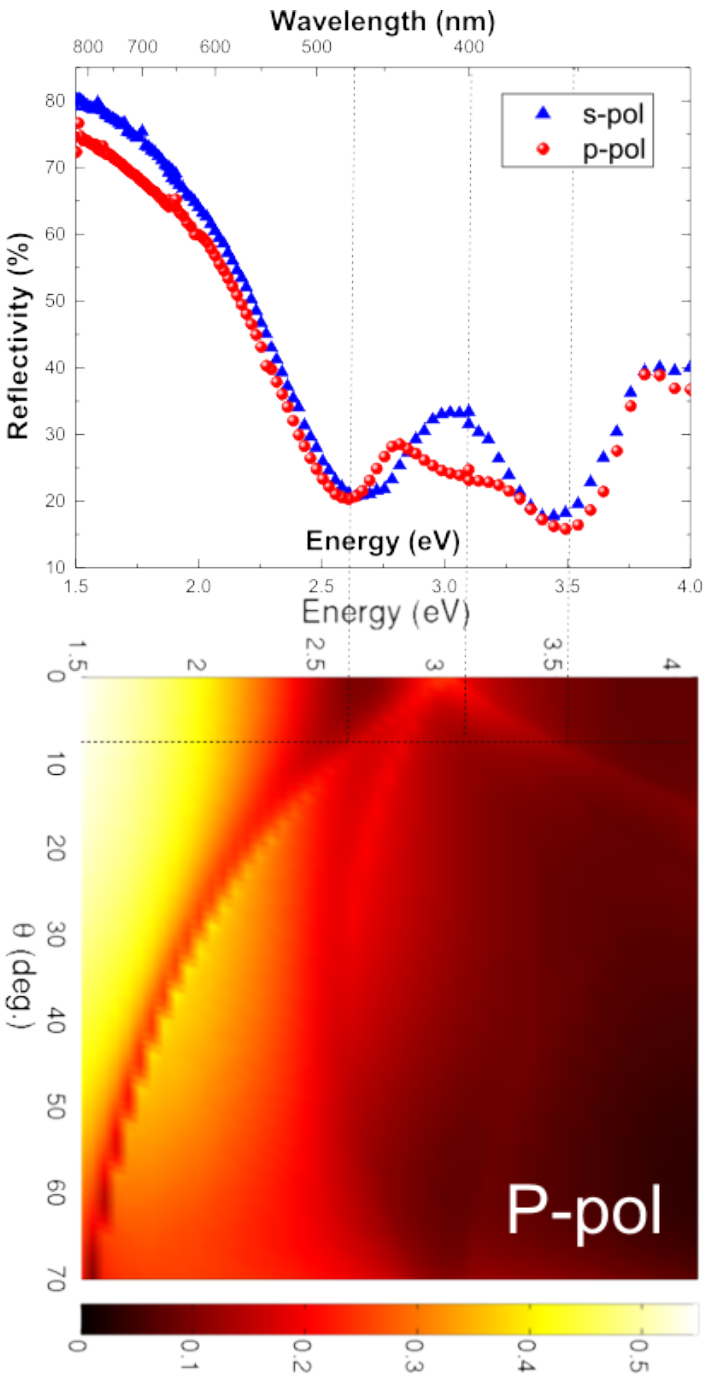

Figure 1: (Upper panel) Reflectivity curves as a function of energy for the anti-dot Ni film with a = 470 nm and d = 275 nm. Measurements performed with for s- and p-polarized light. The data have been normalized to the reflectivity of a Ni continuous film. (Lower panel) Calculated dispersion relation of Bragg plasmons a the Ni-air interface as a function of angle of incidence for p-polarized light and plane of incidence parallel to the nearest neighboor direction of the hexagonal lattice.

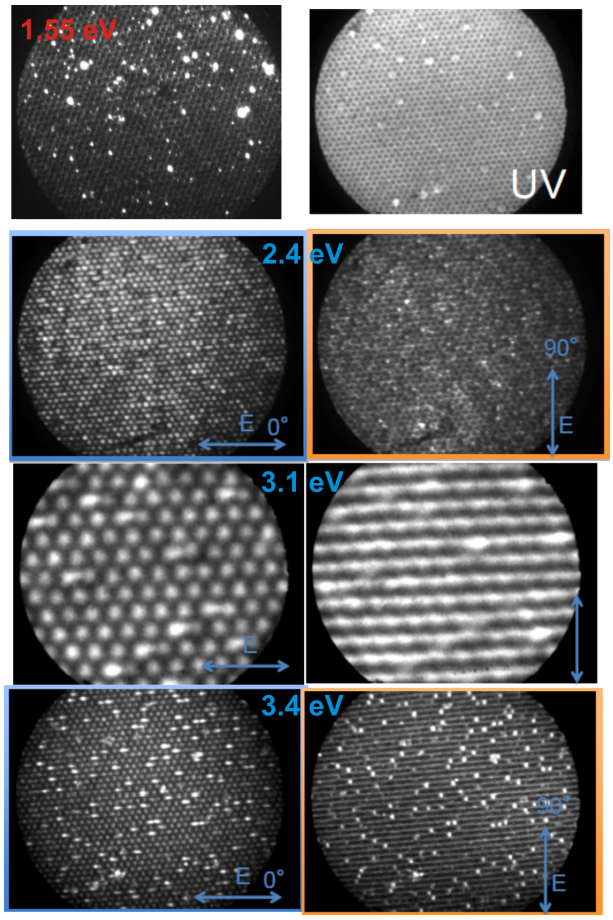

Figure 2: PEEM images of the nickel antidot film under study. The excitation is performed with linear polarized laser light of energies of (1,55 and UV) for the top two images and for 2.4, 3.1 and 3.4 eV as indicated in the next three rows. The laser light is impinging the sample under an angle of incidence of ≤ 4 to the surface normal. The light polarization is changed with a retardation plate (half wave plate). For 2.4 eV not significant changes are observed. For 3.1 and 3.4 eV spot like emission is observed from the region in between the holes when the incident E-vector (p-pol light) is parallel to the shortest direction between the holes. On the other side, when s-light is used and the E-vector is parallel to the next nearest neighbours ΓM direction then we observe the emission that forms lines perpendicular to E-vector direction.

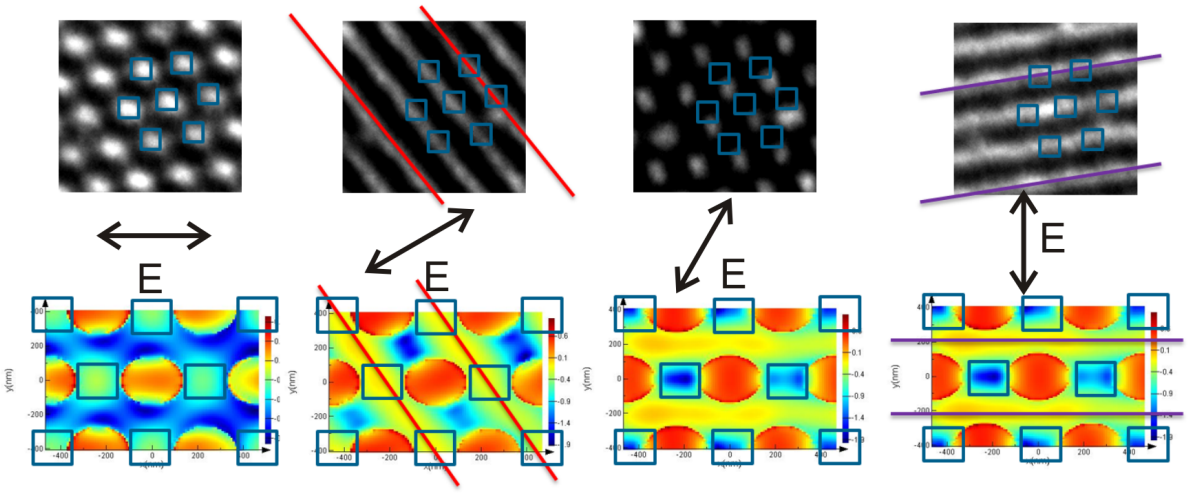

Figure 3: (Upper panel) Experimental photo-emission patterns recorded at 3.1 eV for different polarization states as indicated. (lower panel) Simulated near-field distribution for different polarization states. A very good agreement between the PEEM measurements and the near-field simulations is observed.

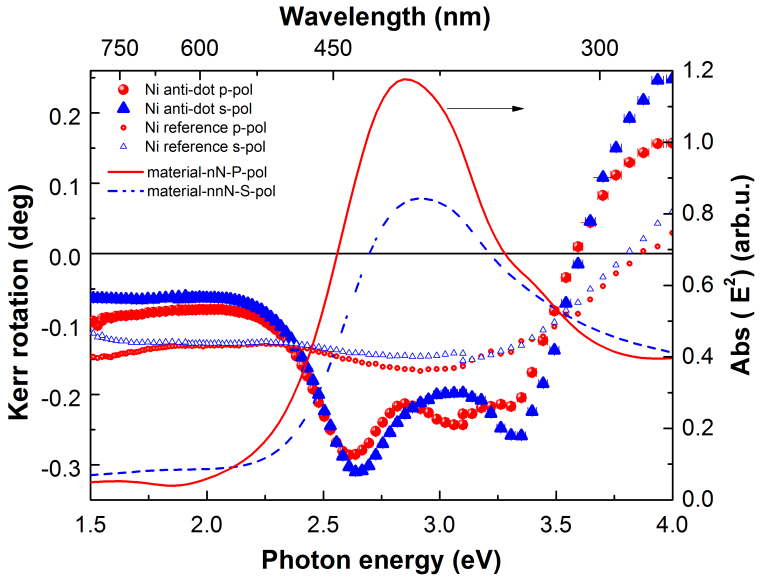

Figure 4: (left axis)Polar Kerr rotation spectra of the Ni anti-dot and a Ni continuous film used as a reference. Measurements performed with for s- and p-polarized light for both samples at the magnetic saturation of the samples at B= 1T. (right axis)Absolute value of the electric field intensities calculated from the simulated patterns in Fig. 3